

When does vapor pressure deficit drive or reduce evapotranspiration?

A. Massmann¹, P. Gentine¹, C. Lin²

⁴¹Department of Earth and Environmental Engineering, Columbia University, New York, NY 10027

⁵²Department of Hydraulic Engineering, Tsinghua University, Beijing, CN

Key Points:

- ⁷ • = enter point 1 here =
- ⁸ • = enter point 2 here =
- ⁹ • = enter point 3 here =

10 **Abstract**

11 = enter abstract here =

12 **1 Introduction**

13 Changes to vapor pressure deficit (VPD) alter the atmospheric demand for water from
 14 the land surface. However, plant stomata have evolved to optimally regulate the exchange of
 15 water and carbon between vegetation and the atmosphere [Franks *et al.*, 2017]. Therefore, an
 16 increase (decrease) in VPD may not correspond to an increase (decrease) in evapotranspiration
 17 (ET) because stomatal closure (opening) can cancel the effects of shifts to atmospheric
 18 demand.

← This section
needs to be
fleshed out,
and I defi-
nitely need
to add more
citations

19 Quantifying the plant response to a perturbation to atmospheric VPD increases our
 20 understanding of feedbacks between the land surface and the atmosphere. If plant response
 21 reduces ET in response to an increase in VPD, the land surface will contribute a positive
 22 feedback in response to atmospheric drying. Conversely, if plant response increases ET in
 23 response to increase in VPD, then the land surface will contribute a negative feedback to
 24 atmospheric drying. The sign of these feedbacks drives the evolution of the atmosphere and
 25 land-surface at many timescales, from diurnal to interdecadal.

26 Here we use a Penman-Monteith framework to quantify plant response to perturbations
 27 to atmospheric demand for water. Section 2 derives the framework, Section 3 describes the
 28 data used, Section 4 presents results, and Section 5 discusses conclusions. The goal of this
 29 paper is to use reasonable approximations as a tool to increase intuition for plant response to
 30 atmospheric drying. This intuition will aid interpretation of observations and full complexity
 31 climate models.

32 **2 Methods**

33 The Penman-Monteith equation (hereafter PM) estimates ET as a function of atmo-
 34 spheric and land-surface variables:

$$ET = \frac{\Delta R + g_a \rho_a c_p D_s}{\Delta + \gamma(1 + \frac{g_a}{g_s})}, \quad (1)$$

36 where variable definitions are given in Table 1. *MEDLYN et al.* [2011] developed a
 37 model for g_s by combining optimal photosynthesis theory with empirical approaches. The
 38 result for leaf-scale stomatal resistance was:

$$39 \quad g_{l-s} = g_0 + 1.6 \left(1 + \frac{g_1}{\sqrt{D_s}} \right) \frac{A}{c_s} \quad (2)$$

40 This can be adapted to an ecosystem-scale stomatal resistance by multiplying by leaf
 41 area index (LAI) and converting units to m s^{-1} :

$$42 \quad g_s = \text{LAI} \frac{R * T}{P} \left(g_0 + 1.6 \left(1 + \frac{g_1}{\sqrt{D_s}} \right) \frac{A}{c_s} \right) \quad (3)$$

43 While Equation 3 can be used in PM, it will make analytical work with the function
 44 intractable because A is a relatively strong function of ET. To remove dependence of ET on A
 45 we can use the semi-empirical results of *Zhou et al.* [2015]. *Zhou et al.* [2015] showed that:

$$46 \quad uWUE = \frac{GPP \cdot \sqrt{D}}{ET} \quad (4)$$

47 is relatively constant across time and space (within plant functional type). If, following *Lin*
 48 *et al.* [2015], we approximate g_0 as 0, we can use uWUE to remove A from g_s in a way that
 49 makes PM analytically tractable:

$$50 \quad g_s = \text{LAI} \frac{R * T}{P} 1.6 \left(1 + \frac{g_1}{\sqrt{D_s}} \right) \frac{uWUE \cdot ET}{c_s \sqrt{D}} \quad (5)$$

51 Plugging Equation 5 into Equation 1 and rearranging gives:

$$52 \quad ET = \frac{\Delta R + \frac{g_a P}{T} \left(\frac{c_p D_s}{R_{air}} - \frac{\gamma c_s \sqrt{D}}{\text{LAI} R * 1.6 uWUE (1 + \frac{g_1}{\sqrt{D}})} \right)}{\Delta + \gamma} \quad (6)$$

53 We can then take the derivative with respect to D to determine ecosystem response to
 54 atmospheric demand perturbations:

$$55 \quad \frac{\partial ET}{\partial D} = \frac{g_a P}{T(\Delta + \gamma)} \left(\frac{c_p}{R_{air}} - \frac{\gamma c_s}{\text{LAI} 1.6 R uWUE} \left(\frac{2g_1 + \sqrt{D}}{2(g_1 + \sqrt{D})^2} \right) \right) \quad (7)$$

56 Note that given yearly uWUE from *Zhou et al.* [2015], g_1 from *Lin et al.* [2015] [as presented
 57 in *Franks et al.*, 2017], and observations of R, T, P, D_s , and wind speed (WS), the only un-

65

Table 1. Definition of symbols and variables

| Variable | Description | Units |
|-----------|--|---|
| e_s | saturation vapor pressure | Pa |
| T | temperature | K |
| Δ | $\frac{\partial e_s}{\partial T}$ | Pa K^{-1} |
| R | net radiation at land surface minus ground heat flux | W m^{-2} |
| g_a | atmospheric conductance | m s^{-1} |
| ρ_a | air density | kg m^{-3} |
| c_p | specific heat capacity of air at constant pressure | $\text{J K}^{-1} \text{ kg}^{-1}$ |
| D | VPD | Pa |
| γ | psychrometric constant | Pa K^{-1} |
| g_s | stomatal conductance | m s^{-1} |
| g_{l-s} | leaf-scale stomatal conductance | $\text{mol m}^{-2} \text{ s}^{-1}$ |
| R^* | universal gas constant | $\text{J mol}^{-1} \text{ K}^{-1}$ |
| LAI | leaf area index | - |
| c_s | CO_2 concentration | $\mu \text{ mol CO}_2 \text{ mol}^{-1} \text{ air}$ |

^aFootnote text here.

58

known is LAI. With flux tower observations of ET, LAI will then be uniquely determined for each observation through Equation 6:

59

60

$$LAI = -\frac{g_a \gamma c_s \sqrt{D_s} P}{(\text{ET} (\Delta + \gamma) - \Delta R - g_a \rho_a c_p D_s) 1.6 R T \text{ uWUE} (1 + \frac{g_l}{\sqrt{D_s}})} \quad (8)$$

61

This “pseudo-LAI” is some part “true” LAI (a measure of leaf area), and some part model and observational error, including error involving our assumption of constant uWUE. By calculating a unique LAI for each observation we will propagate any model and observational uncertainty forward into our expression for $\frac{\partial ET}{\partial D}$.

62

63

64

70 **Table 2.** Plant functional types, their abbreviation, Medlyn coefficient [from *Lin et al.*, 2015], and uWfUE
 71 [from *Zhou et al.*, 2015]. Note that units are converted such that the quantities fit into Equations 1-8 with the
 72 variables in Table 1.

| Abbreviation | PFT | g_1 ($\text{Pa}^{0.5}$) | uWUE ($\mu\text{-mol [C]} \text{ Pa}^{0.5} \text{ J}^{-1} [\text{ET}]$) |
|--------------|-----------------------------|-----------------------------|---|
| CRO | cropland | 183.1 | 3.80 |
| CSH | closed shrub | 148.6 | 2.18 |
| DBF | deciduous broadleaf forest | 140.7 | 3.12 |
| ENF | evergreen needleleaf forest | 74.3 | 3.30 |
| GRA | grassland (C3) | 166.0 | 2.68 |

“Footnote text here.

66 **3 Data**

67 We use data from FLUXNET2015. Because g_1 coefficients [*Lin et al.*, 2015] and uWUE
 68 were only both available for five plant functional types (PFTs - see Table 2), only 56 of the 77
 69 sites were used. Figure 1 presents each site and its plant functional type.

70 We restrict our analysis to the daytime (sensible heat $> 5 \text{ W m}^{-2}$ and shortwave radia-
 71 tion $> 50 \text{ W m}^{-2}$) when there is no precipitation and the plants are growing (GPP $> 10\%$ of
 72 the 95th percentile). Also, because some sites use half hourly data but some use hourly, we
 73 aggregate all data to hourly averages. Only times with good quality control flags are used.

← map needs
to be im-
proved - it's
a placeholder
for now

← This GPP
thresholding
was used by
Changjie, do
you know if
there is a ci-
tation for it?
Otherwise it
seems like
something a
reviewer
would have
issue with as
it is arbitrary

79 **4 Results**

80 By construction, the variability in the LAI term (Equation 8) contains all model and
 81 observational uncertainties. LAI also has physical meaning corresponding to “true” leaf area,
 82 and we expect that it would be approximately $O(1)$, especially because uWUE is fit in *Zhou*
 83 *et al.* [2015] at the ecosystem-level. We can have some confidence in our framework, in-
 84 cluding the assumption of constant uWUE, if calculated LAIs are generally $O(1)$. Figure 2
 85 presents the histogram of calculated LAIs with outliers (lowest and highest 5% percent) and
 86 nonphysical values ($\text{LAI} < 0$) removed. All remaining LAI values are $O(1)$ which provides
 87 confidence in model framework.

91 An additional concern is that the LAI term may in fact be some function of D , in which
 92 case the dependence would need to be accounted for when taking the derivative. Figure 3.
 93 plots the joint distribution of LAI and VPD, and shows that LAI is very weakly a function of
 94 VPD. Given this weak dependence, we argue that Equation 7 is a valid approximation for ET
 95 response to D .

← Figs 2 and 3
 can probably
 be combined
 - the his-
 togram of
 LAI is shown
 in Fig 3

100 Before diving into calculated values of $\frac{\partial ET}{\partial D}$, it is useful to consider the functional
 101 form of Equation 7. There are three terms: a scaling term for the full expression we will call
 102 Term 1 ($\frac{g_a P}{T(\Delta+\gamma)}$), a relatively constant offset we will call Term 2 ($\frac{c_p}{R_{air}}$), and a variable term
 103 we will call Term 3 ($\frac{\gamma c_s}{LAI 1.6 R \text{ uWUE}} \left(\frac{2g_1 + \sqrt{D}}{2(g_1 + \sqrt{D})^2} \right)$). All variables are positive, so the relative
 104 magnitude between Term 2 and Term 3 will determine the sign of the derivative, while Term
 105 1 will scale the expression larger or smaller.

106 In Term 1, $\frac{P}{T} \propto \rho$, so this should vary little relative to g_a and Δ . γ should also be rel-
 107 atively constant. So the scaling term, Term 1, should be primarily a function of g_a and tem-
 108 perature (through the function Δ). While temperature range may vary for PFT, the functional
 109 form of Δ will be the same. g_a will vary strongly with PFT due to the importance of surface
 110 roughness. However, the coefficient of variability for both g_a and Term 1 is relatively con-
 111 stant across PFT, suggesting that the influence of g_a on the relative (to the mean) variability
 112 of Term 1 is approximately similar across PFT.

113 Figure 4A shows Term 1 normalized by mean g_a (calculated for each plant functional
 114 type), and confirms that much of the relative variability of Term 1 is contained in the g_a
 115 term's relative variability. Generally, T has less of a role. Additionally, the impact of T on
 116 the relative variability increases with increasing g_a .

117 While the relative variability of Term 1 is similar across PFT, the absolute value of
 118 Term 1 varies strongly across PFT. Figure 4B shows Term 1 evaluated with the mean g_a for
 119 each PFT, and at the range of observed temperatures for each PFT. As expected, for the tree
 120 PFTs (DBF, ENF) Term 1 is much larger and the temperature dependence is much stronger.
 121 Systematic differences in observed temperatures also cause differences in the average mag-
 122 nitude of Term 1. For example, ENF experiences on average colder temperatures and is thus
 123 more likely to have a larger scaling term. Additionally, because $\text{std}(g_a) \propto \overline{g_a}$, the spread of
 124 Term 1 due to g_a variability will be larger for the tree PFTs, although this is not shown for
 125 simplicity. To summarize, the variability of Term 1 within each PFT will look like Figure 4A

126 for each PFT, but the scale of the x and y-axis will increase or decrease according to mean g_a
 127 observed in Figure 4B.

132 Term 2 minus Term 3 determines the sign and magnitude that the scaling Term 1 is
 133 multiplied by. If we assume that c_s variability is relatively less than LAI and D variability,
 134 then variability within PFT will be solely determined by LAI and D . Figure 5 shows how
 135 (Term 2 - Term 3) varies with D and LAI, as a function of PFT. In Figure 5a lower uWUE
 136 and LAI shift the distribution of (Term 2 - Term 3) towards negative values. Additionally, the
 137 smaller g_1 , the greater the relative D dependence of (Term 2 - Term 3). This is observed
 138 most strongly for the ENF PFT, which has the smallest g_1 (74.31).

145 Figure 5b shows the location of the minima of ET, as a function of LAI and D . For any
 146 LAI or VPD less (more) than these curves, Term 2 - Term 3 will be negative (positive). It is
 147 clear that the portion of VPD observations below/above these curves will be a strong func-
 148 tion of LAI. However, we can see some general trends. For CSH, $\frac{\partial ET}{\partial D}$ should be negative
 149 for the vast majority of observed LAI and VPD. The split appears to be more even among
 150 ENF, GRA, and DBF, and we might expect a greater frequency of positive $\frac{\partial ET}{\partial D}$ for CRO.

151 Table 3 confirms these expectations for PFT behavior of $\frac{\partial ET}{\partial D}$. For all PFTs except
 152 for CRO, average $\frac{\partial ET}{\partial D}$ is less than zero. However, $\frac{\partial ET}{\partial D}$ evaluated at the average of all vari-
 153 ables (e.g. LAI, T , c_s , D) is only negative for CSH and GRA. And, DBF in addition to CRO
 154 experiences $\frac{\partial ET}{\partial D} < 0$ less than half the time. These observations highlight the effect of the
 155 nonlinear function in Figure 5: $\frac{\partial ET}{\partial D}$ has a much steeper slope when the function is negative,
 156 and is thus more likely to be large magnitude.

157 The units of $\frac{\partial ET}{\partial D}$ make it difficult to interpret if D is even a meaningful contributor to
 158 ET's variability. To understand D 's contribution better, we use a linear approximation and
 159 present $\frac{\partial ET}{\partial D}$ multiplied by D 's standard deviation. The D 's contribution to ET's variabil-
 160 ity ranges between 16 - 20 W m⁻² for all PFTs except for CSH, which is about 51 W m⁻².
 161 Another meaningful comparison is to $\frac{\partial ET}{\partial R} * std(R)$, as net radiation generally the driver of
 162 ET (cite joe berry here). For all PFTs except for CSH D contributes between 14.5 - 20.5 %
 163 of R 's contribution to variability. For CSH the portion is much larger, about 44 %. However
 164 it is important to note that a linear approximation about a mean base state is probably not a
 165 very good approximation across the range of variability, so these values are just estimates of
 166 D 's contribution to ET's variability. Regardless, D 's variability is certiantly a non-negligable
 167 contributor to ET's variability.

181

Table 3. Statistics of $\frac{\partial ET}{\partial D}$ as a function of PFT.

| PFT | $\overline{\frac{\partial ET}{\partial VPD}}$ | $\overline{\frac{\partial ET}{\partial D}}(\overline{T}, \dots, \overline{D})$ | $\overline{\frac{\partial ET}{\partial D}}(\overline{T}, \dots, \overline{D}) * \text{std}(D)$ | $\frac{\overline{\frac{\partial ET}{\partial D}}(\overline{T}, \dots, \overline{D}) * \text{std}(D)}{\overline{\frac{\partial ET}{\partial R}}(\overline{T}, \dots, \overline{D}) * \text{std}(R)}$ | fraction $\frac{\partial ET}{\partial VPD} < 0$ |
|-----|---|--|--|---|---|
| CRO | 0.000853 | 0.026241 | 18.523659 | 0.203022 | 0.473311 |
| CSH | -0.108234 | -0.091526 | 50.861613 | 0.439379 | 0.931660 |
| DBF | -0.012727 | 0.013794 | 19.734435 | 0.164241 | 0.461674 |
| ENF | -0.034087 | 0.000706 | 16.611852 | 0.148548 | 0.534425 |
| GRA | -0.019637 | -0.000921 | 16.798083 | 0.173552 | 0.631735 |

^aFootnote text here.

168 So far, idealized plots and statistics have illuminated the form of $\frac{\partial ET}{\partial D}$ and how it varies
 169 with PFT. Large mean LAI and uWUE shifts CRO and DBF towards positive $\overline{\frac{\partial ET}{\partial D}}$. How-
 170 ever, the strongly nonlinear function of $\frac{\partial ET}{\partial D}$ at $\frac{\partial ET}{\partial D} < 0$ pushes $\overline{\frac{\partial ET}{\partial D}}$ negative for DBF (it
 171 does not do this for CRO because of CRO's high g_1). ENF's low g_1 value increases the de-
 172 pendence of $\frac{\partial ET}{\partial D}$ on D , and makes the function more strongly nonlinear. This has the side
 173 effect of pushing $\overline{\frac{\partial ET}{\partial D}}$ negative further than other PFTs for a given fraction $\frac{\partial ET}{\partial D} < 0$ and
 174 magnitude $\overline{\frac{\partial ET}{\partial D}}(\overline{T}, \dots, \overline{D})$. GRA shows the opposite behavior; a relatively high g_1 makes
 175 the function more linear, decreasing the magnitude of $-\overline{\frac{\partial ET}{\partial D}}$ for a given [large] fraction
 176 $\frac{\partial ET}{\partial D} < 0$ and negative $\overline{\frac{\partial ET}{\partial D}}(\overline{T}, \dots, \overline{D})$ (although g_a and Term 1 also probably have a role in
 177 this). Finally, low uWUE of CSH pushes toward by far the lowest values $\frac{\partial ET}{\partial D}$ (Figure 5).
 178 Variability in D accounts for the largest about of ET variability for CSH. For the other PFTs,
 179 D contributes less to ET variability, but still represents about 15-20 % of R 's contributions
 180 to ET variability.

182 4.1 Full observations of $\frac{\partial ET}{\partial D}$

183 Now that we have an intuitive understanding of $\frac{\partial ET}{\partial D}$'s behavior, we are equipped to
 184 interpret fully realistic plots of $\frac{\partial ET}{\partial D}$ for each PFT. Figure 6 presents calculated $\frac{\partial ET}{\partial D}$ where,
 185 unless otherwise noted, all variables in Equation 7 are allowed to vary. Each column is a
 186 different quantity related to $\frac{\partial ET}{\partial D}$, and each row is a different PFT.

187 The full observations generally confirm expectations from Section 4. CRO has the
 188 most positive values of $\frac{\partial ET}{\partial D}$, $\overline{\frac{\partial ET}{\partial D}}$ is almost always negative for CSH, and response depends
 189 more with the environmental conditions for the other PFTs (especially ENF). Through the

190 columns of Figure 6 we can see the impact of LAI and g_a on the variability of $\frac{\partial ET}{\partial D}$. g_a 's
 191 scaling (included in columns 1 and 3) alters the magnitude considerably. LAI variability
 192 (included in columns 1 and 2) adds a lot of additional noise to the signal of $\frac{\partial ET}{\partial D}$, which is
 193 slightly undesirable given LAI's role in representing model and observational uncertainty.
 194 However, the general story with the noise appears to match the cleaner signal when LAI is
 195 help constant and D_{ETmin} is clearly visible . One exception is possibly with GRA, for which
 196 uncertainty represented in LAI is high and causes the full complexity plots (Columns 1 and
 197 2) to not match well with LAI held fixed (Columns 3 and 4).

← I really need
to make
these plots
better - way
too much
overlapping
of points
that hurts
the story

198 For ENF and GRA D_{ETmin} does not appear to be only a function of LAI (most observ-
 199 able in Column 4). It turns out that the site to site variability in γ causes D_{ETmin} to vary,
 200 which is not discussed in the previous section. The impact is observable in both ENF and
 201 GRA, but especially for ENF which has a larger $\frac{\partial^2 ET}{\partial^2 D}$ than the other PFTs.

207 In general the full complexity plots of $\frac{\partial ET}{\partial D}$ match our expectations, even with the large
 208 sensitivity to LAI measures of uncertainty observed in Figure 5. Our LAI-based method of
 209 uncertainty propagation blurs the idealized expectations the most for GRA, and also has a
 210 considerable effect for CRO. We therefor have the most confidence in our conclusion based
 211 on Equation 7 for PFTS CSH, DBF, and ENF, as the full complexity plots with uncertainty
 212 included closely match the story when LAI is held fixed. **see somewhat preferred alternate
 213 figure 7 .

← I think I like
the alternate
plot much
more as
thinking in
terms of T
and RH is
easier, and
it makes the
story easier
to see at rel-
atively low
temperatures.

217 5 Conclusions

218 The idealized representation of ET used here is successful in developing intuition for
 219 how ET responds to changes in D . This intuition will aid the community in interpreting ob-
 220 servations and output from sophisticated full complexity climate models.

221 The idealized framework leads to the following general conclusions:

- 222 • Aerodynamic resistance plays an important role of scaling $\frac{\partial ET}{\partial D}$. This is a leading
 223 order effect for observing higher magnitude responses in DBF and ENF.
- 224 • In general, CSH has the most negative (i.e. ET reduced) response to increases in D
 225 (atmospheric drying). So CSH plants will almost always try and conserve water, ef-
 226 fectively reducing ET with dry atmospheric perturbation.
- 227 • Additionally for CSH, D variability contributes the most to ET variability.

← I think I like
the alternate
plot much
more as
thinking in
terms of T
and RH is
easier, and
it makes the
story easier
to see at rel-
atively low
temperatures.
However,
I used the
other plot be-
cause Fig 5
does not dis-
cuss things
in terms of
temperature,
as this would
make things
more compli-
cated (adding
another di-
mension).
I could just
include both
versions
of figure 6
though (us-
ing figure 6a
as a bridge to
figure 6b)

- CRO has the most positive response (i.e. ET increased) in response to increases in *D*. This is consistent with CROs that may be evolved or bred to thrive in non-water-limited environments.
- The response is more a function of the environment for DBF, ENF, and GRA. Because as VPD increases the response is more likely to be positive, if RH is fixed then the response will be more likely to be positive at warmer T, or if T is fixed the response is more likely to be positive with decreasing RH.
- ENF has the strongest dependence on environmental conditions due to its small g_1 .
- Model and observational uncertainty is highest for GRA and CRO, so conclusions about those PFTs should be tempered.
- However, inclusion of uncertainty doesn't alter conclusions about DBF, ENF, and CSH.

The intuition developed using this framework can be used to understand how the land surface will respond and contribute to changes in the environment.

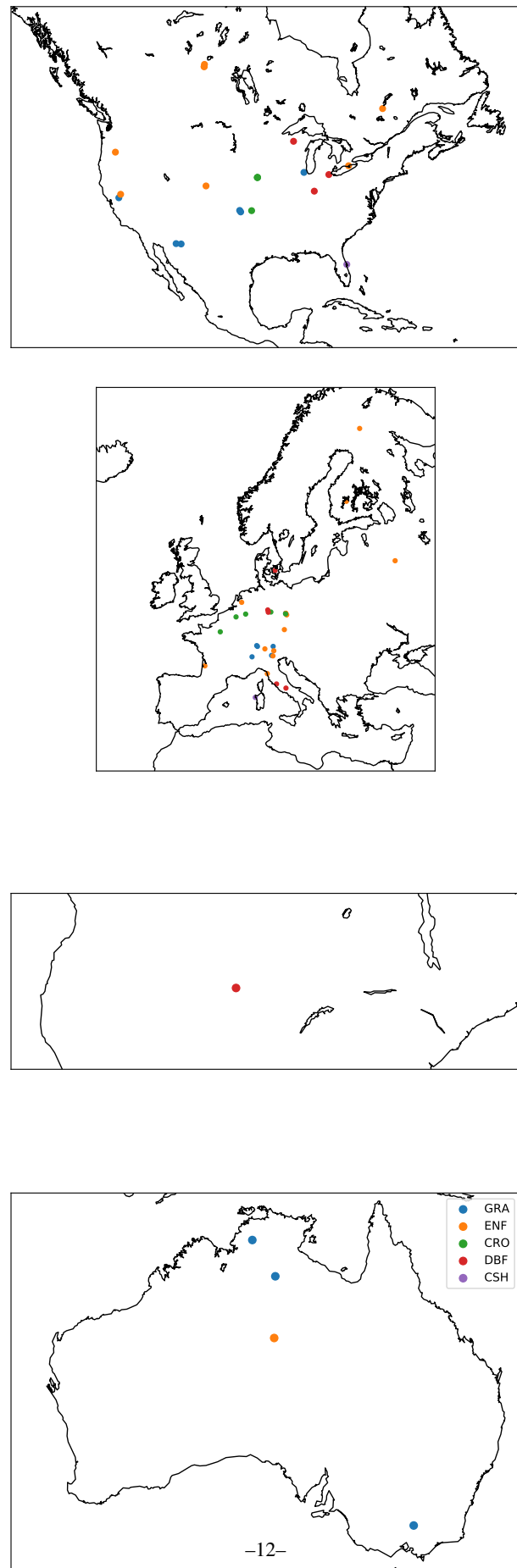
Acknowledgments

This work used eddy covariance data acquired and shared by the FLUXNET community, including these networks: AmeriFlux, AfriFlux, AsiaFlux, CarboAfrica, CarboEuropeIP, CarboItaly, CarboMont, ChinaFlux, Fluxnet-Canada, GreenGrass, ICOS, KoFlux, LBA, NECC, OzFlux-TERN, TCOS-Siberia, and USCCC. The ERA-Interim reanalysis data are provided by ECMWF and processed by LSCE. The FLUXNET eddy covariance data processing and harmonization was carried out by the European Fluxes Database Cluster, AmeriFlux Management Project, and Fluxdata project of FLUXNET, with the support of CDIAC and ICOS Ecosystem Thematic Center, and the OzFlux, ChinaFlux and AsiaFlux offices.

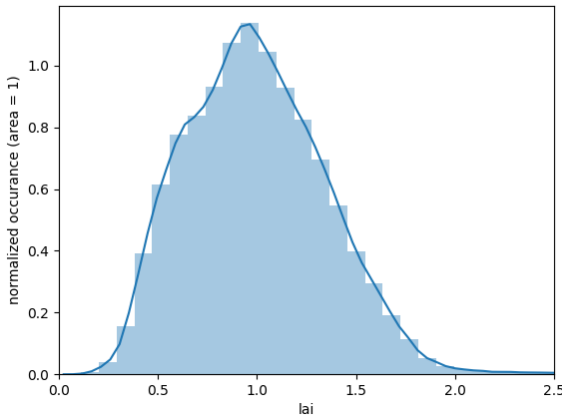
References

- Franks, P. J., J. A. Berry, D. L. Lombardozzi, and G. B. Bonan (2017), Stomatal function across temporal and spatial scales: Deep-time trends, land-atmosphere coupling and global models, *Plant Physiology*, 174(2), 583–602, doi:10.1104/pp.17.00287.
- Lin, Y.-S., B. E. Medlyn, R. A. Duursma, I. C. Prentice, H. Wang, S. Baig, D. Eamus, V. R. de Dios, P. Mitchell, D. S. Ellsworth, M. O. de Beeck, G. Wallin, J. Uddling, L. Tarvainen, M.-L. Linderson, L. A. Cernusak, J. B. Nippert, T. W. Ocheltree, D. T. Tissue, N. K.

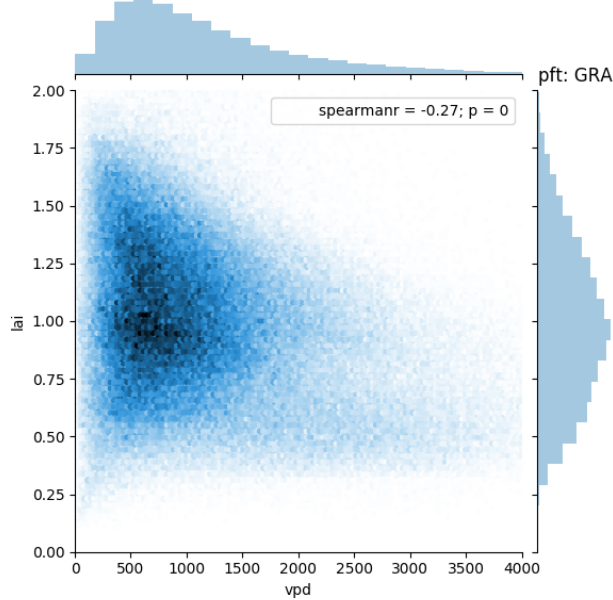
- 258 Martin-StPaul, A. Rogers, J. M. Warren, P. D. Angelis, K. Hikosaka, Q. Han, Y. Onoda,
259 T. E. Gimeno, C. V. M. Barton, J. Bennie, D. Bonal, A. Bosc, M. LÃºw, C. Macinins-
260 Ng, A. Rey, L. Rowland, S. A. Setterfield, S. Tausz-Posch, J. Zaragoza-Castells, M. S. J.
261 Broadmeadow, J. E. Drake, M. Freeman, O. Ghannoum, L. B. Hutley, J. W. Kelly,
262 K. Kikuzawa, P. Kolari, K. Koyama, J.-M. Limousin, P. Meir, A. C. L. da Costa, T. N.
263 Mikkelsen, N. Salinas, W. Sun, and L. Wingate (2015), Optimal stomatal behaviour
264 around the world, *Nature Climate Change*, 5(5), 459–464, doi:10.1038/nclimate2550.
- 265 MEDLYN, B. E., R. A. DUURSMA, D. EAMUS, D. S. ELLSWORTH, I. C. PRENTICE,
266 C. V. M. BARTON, K. Y. CROUS, P. D. ANGELIS, M. FREEMAN, and L. WINGATE
267 (2011), Reconciling the optimal and empirical approaches to modelling stomatal conduc-
268 tance, *Global Change Biology*, 17(6), 2134–2144, doi:10.1111/j.1365-2486.2010.02375.x.
- 269 Zhou, S., B. Yu, Y. Huang, and G. Wang (2015), Daily underlying water use efficiency for
270 AmeriFlux sites, *Journal of Geophysical Research: Biogeosciences*, 120(5), 887–902, doi:
271 10.1002/2015jg002947.



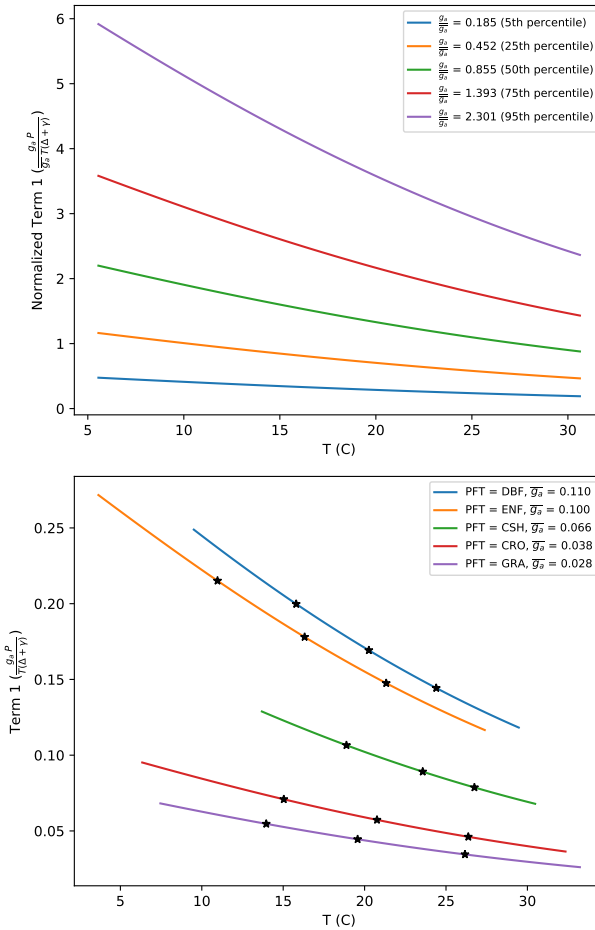
73 **Figure 1.** Plant functional type and location of sites used in analysis. ***This is just a placeholder for now
74 and needs to be improved i.e. with lat lon, better placement of continents, etc.)***



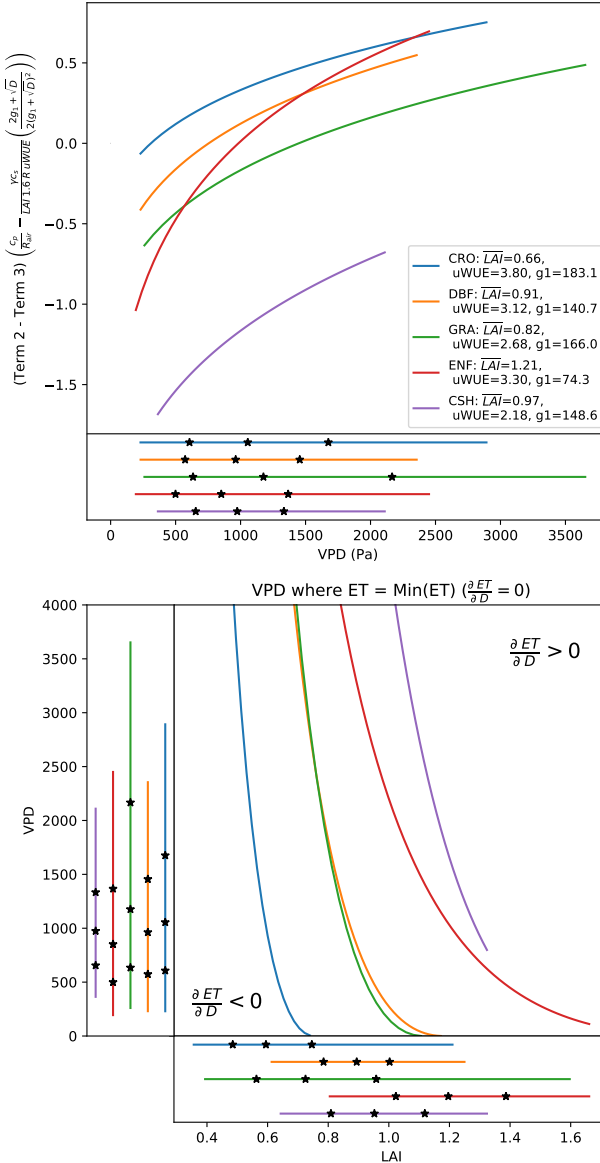
88 **Figure 2.** Histogram of LAI values calculated for each site and time according to Equation 8.
 89 The lowest and highest 5% are removed as outliers, as well as any values below 0. The curve is normalized such that its
 90 area is 1.



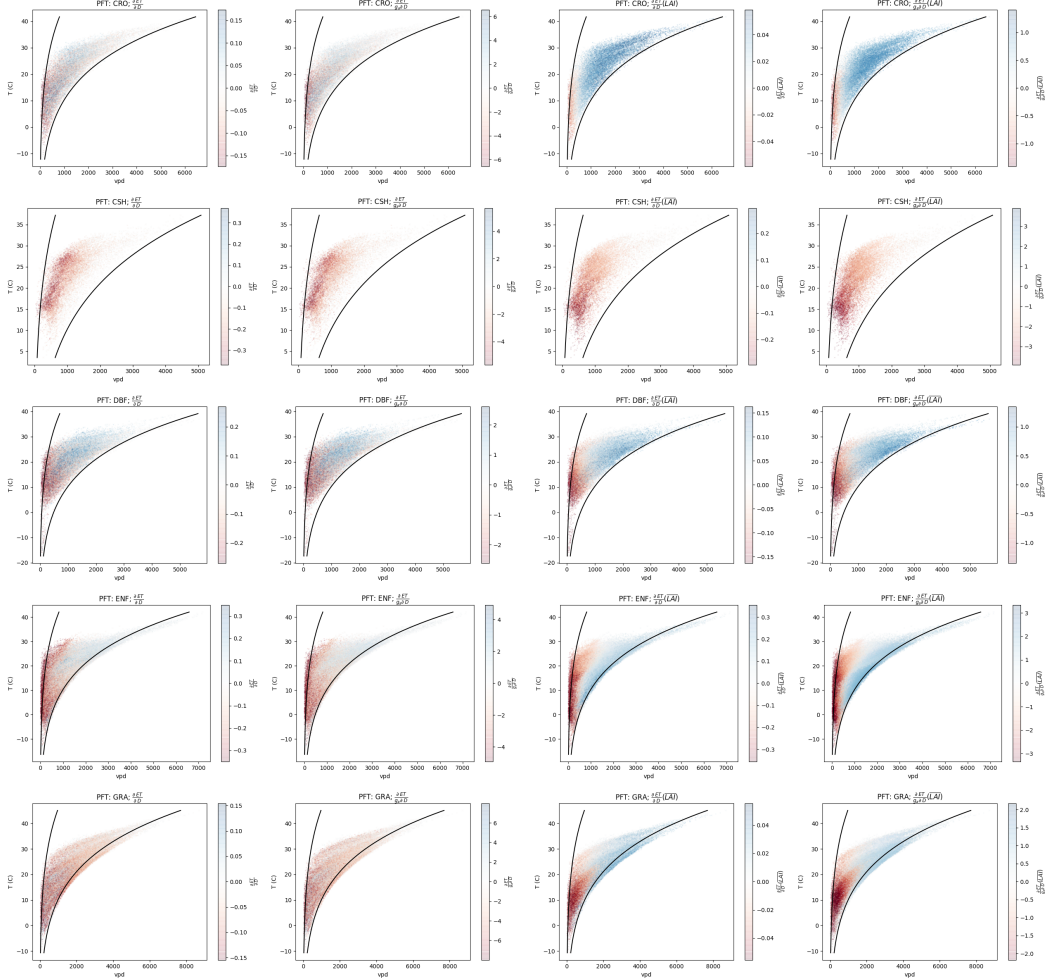
96 **Figure 3.** The joint distribution of D and LAI. LAI has only a weak dependence on D . ***This plot
 97 could probably benefit from a box plot of site specific correlations, because some sites do have stronger
 98 dependence than others. Note also Figs 3 and 2 can probably be combined because this figure shows LAI's
 99 histogram.***



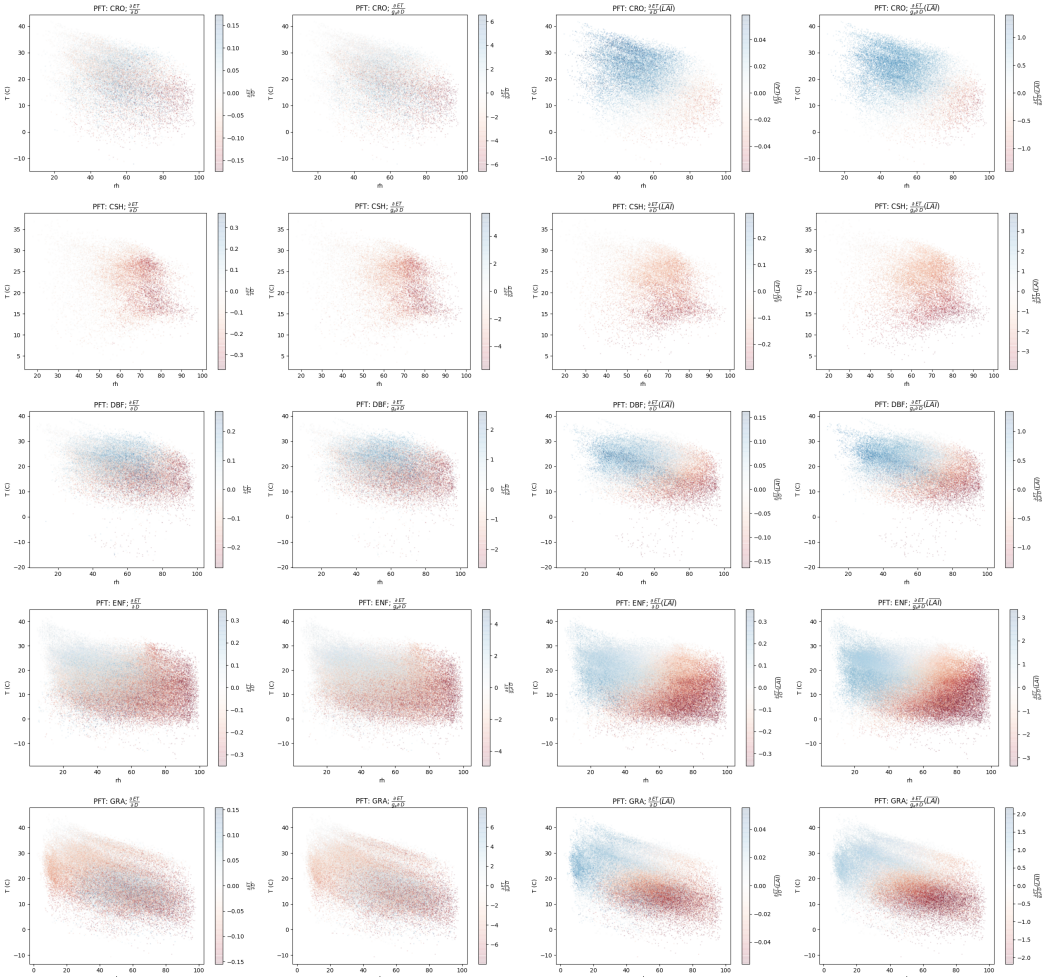
128 **Figure 4.** Primary sources of variability for Term 1. A) Variability within each PFT: Term 1 normalized by
 129 mean g_a for each PFT. B) Variability between each PFT: Term 1 evaluated at mean g_a for each PFT. Tempera-
 130 ture range is 5-95th percentile for each PFT. Additionally, stars denote the location of the 25th, 50th, and 75th
 131 percentiles.



139 **Figure 5.** Sources of variability for Term 2 - Term 3. Top: Term 2 - Term 3 as a function of VPD, with
 140 LAI held fixed at PFT averages. The observed range of VPD for each PFT is also shown below the x-axis.
 141 Line extent corresponds to 5th and 95th percentiles, while stars denote the location of the 25th, 50th, and 75th
 142 percentiles.
 143 Bottom: The location of the minima of ET, as a function of VPD and LAI. Lines and stars denote the distribu-
 144 tion of VPD and LAI next to each axis, following the same percentiles as above.



202 **Figure 6.** Scatter plots of $\frac{\partial ET}{\partial D}$. Each row is a different PFT, and each column is a different quantity related
 203 to $\frac{\partial ET}{\partial D}$, as labeled: Column 1 - $\frac{\partial ET}{\partial D}$; Column 2 - $\frac{\partial ET}{\partial D}$ normalized by g_a ; Column 3 - $\frac{\partial ET}{\partial D}$ with LAI held
 204 fixed at PFT average; and Column 4 - $\frac{\partial ET}{\partial D}$ normalized by g_a and with LAI held fixed. For reference, lines
 205 corresponding to RH = 20% and RH = 90 % are drawn. Please note differences in the colorbar scale. ***see
 206 alternate (or additional) plot below.***



214 **Figure 7.** ****alternate Fig 06**** Scatter plots of $\frac{\partial ET}{\partial D}$. Each column
 215 is a different quantity related to $\frac{\partial ET}{\partial D}$, as labeled. If I end up using this, I could also draw on the curve of
 216 D_{ETmin} with \overline{LAI} .